Journal of Materials Chemistry C

Incorporation of Fluorescent Quantum Dots for 3D Printing and Additive Manufacturing Applications

Journal:	*Journal of Materials Chemistry C*
Manuscript ID	TC-ART-04-2018-002024.R1
Article Type:	Paper
Date Submitted by the Author:	26-Jun-2018

Complete List of Authors:	Brubaker, Cole; Vanderbilt University, Civil and Environmental Engineering Frecker, Talitha; Vanderbilt University, Chemistry McBride, James; Vanderbilt University, Chemistry Reid, Kemar; Vanderbilt University, Interdisciplinary Materials Science Jennings, Kane G; Vanderbilt University, Chemical and Biomolecular Engineering Rosenthal, Sandra; Vanderbilt University, Chemistry Adams, Douglas; Vanderbilt University, Civil and Environmental Engineering

Incorporation of Fluorescent Quantum Dots for 3D Printing and Additive Manufacturing Applications

Cole D. Brubaker,[†,‡] Talitha M. Frecker,[#,‡] James R. McBride,[#] Kemar R. Reid,[§] G. Kane Jennings,[▽] Sandra J. Rosenthal,[#,//,°,§,▽,*] Douglas E. Adams[†,⊥,*]

Departments of [†]Civil and Environmental Engineering, [#]Chemistry, [//] Physics and Astronomy, [°]Pharmacology, [§]Interdisciplinary Materials Science, [▽]Chemical and Biomolecular Engineering, [⊥]Mechanical Engineering, Vanderbilt University, Nashville, Tennessee 37235, United States.

Key Words: 3D printing, additive manufacturing, quantum dot, fluorescent nanoparticle, nanocomposite.

ABSTRACT

In line with the rapid adoption of 3D printing in both industrial and academic fields, the development of functional materials compatible with 3D printing applications represents a promising direction for the continued advancement and adoption of additive manufacturing technologies. Through various materials processing and design considerations, we demonstrate the ability to incorporate cadmium sulfur selenide graded alloy quantum dots (CdSSe QDs) directly within a polylactic acid (PLA) host matrix to obtain nanofunctionalized, fluorescent filament compatible with stock 3D printing systems. Absorbance, photoluminescence, thermal analysis and mechanical testing are studied to quantify how filament functionalization modulates the optical and material properties of the embedded quantum dots and PLA host matrix following

printing. With increasing concentration of embedded quantum dots, a spectral red shift of up to 32 nm relative to CdSSe QDs in solution was observed for 3D-printed PLA/CdSSe QD samples, with the recorded photoluminescence intensity reaching a maximum near a 3%-by-weight loading of CdSSe QDs. Furthermore, the presence of CdSSe QDs within the PLA host matrix was found to influence both the thermal and mechanical response of 3D-printed PLA/CdSSe QD systems. The glass transition temperature was found to decrease by 8°C relative to the unmodified pure PLA host matrix, while ultimate tensile strength decreased by 64% for the highest concentration of CdSSe QDs in PLA tested. We attribute these deviations in material properties to a combination of interactions between the natively bound surface ligands present on CdSSe QDs and PLA host matrix, and quantum dot aggregation in the final 3D-printed structures. Following materials characterization, we demonstrate the ability to 3D print light pipes based on the optical response of embedded CdSSe QDs, where the overall efficiency and performance was found to be dependent on both the physical light pipe dimensions and concentration of embedded quantum dots.

INTRODUCTION

With the ability to shorten production times, while simultaneously minimizing material waste, many industry experts have dubbed additive manufacturing and 3D printing related technologies as the fourth industrial revolution – Industry 4.0 – due to its highly disruptive nature in the manufacturing sector. In order to accelerate product development and minimize manufacturing and production costs (e.g. retooling), additive manufacturing is being used to 3D print a myriad of parts and components for a wide range of products with complex shapes in applications including aircrafts, automobiles, and biomedical implants.[1,2] Utilizing a layer-by-

layer approach, additive manufacturing technologies are typically classified according to the method of deposition and range of compatible materials.[2–4] Material extrusion, powder bed fusion, binder jetting, sheet lamination and vat polymerization are various examples of additive manufacturing approaches currently being used.[4] By utilizing compatible materials including polymers, plastics, metals, ceramics, organic materials and even living cells, a range of products have been fabricated for airplanes and automobiles,[5] manufacturing tooling,[6] electronics,[7] medical devices,[8] and prosthetics.[9] Though each approach has its own set of advantages and drawbacks, fused deposition modeling (FDM), a form of material extrusion, has emerged as one of the most prominent and popular forms of additive manufacturing techniques. The relative affordability of FDM systems, combined with the ease of materials processing and ability to rapidly manufacture functional structures and components, has helped drive the continued demand for FDM related systems and technologies.[10] Similar to other processes where parts and components are 'built up' in a layer-by-layer fashion, FDM utilizes a thermoplastic feedstock to produce the desired part or structure. Here, a polymer-based filament is fed through a nozzle after being heated above its melting temperature and the subsequent molten plastic is deposited onto a build plate. With each layer of material deposited, the printer's build plate is sequentially lowered as the nozzle travels in a predetermined path following the part geometry to manufacture the final structure.

Through materials process and design considerations, the development of new polymer-based materials compatible with material extrusion-based systems has been a recent area of focus in the advancement of FDM technologies. Namely, there has been increasing interest in the development of 'functionalized' materials for additive manufacturing applications. In order

to accomplish this goal, researchers have explored the use of various additives and polymer design/modification to enable 3D-printed materials and structures with a wide range of unique material behaviors and responses. One particular area of research that is gaining tremendous interest is the incorporation of nanomaterials within additive manufacturing processes. On the length scale of approximately 1 – 100 nm, the incorporation of nanomaterials within 3D printing processes can enable a number of new and customizable material behaviors including enhanced material strength properties,[11] increased chemical durability[12] and advanced optical responses[13], among many others, that are not observed in the unmodified host material. Through the proper selection of the nanomaterial system and host matrix, it is feasible to create an array of functionalized nanocomposite systems and materials compatible with additive manufacturing and FDM type processes and applications.

To date, researchers have demonstrated the ability to incorporate a range of organic[14] and inorganic nanomaterial systems including carbon nanotubes,[15] metallic nanoparticles,[16,17] graphene,[18,19] among many others, within the additive manufacturing process. Traditionally, these nanofunctionalized systems are obtained through melt- or solution-mixing processes and extruded to obtain filament compatible with traditional 3D printing systems. In this work, we present a method for the incorporation of fluorescent quantum dots within the additive manufacturing process for FDM-type applications. To the best of our knowledge, this represents the first of such approach for incorporating quantum dots within bulk scale additive manufacturing applications. Their solution processability, wide range of material- and size-dependent properties, and unique optical and emissive characteristics make quantum dots an ideal platform for the development of the next generation of nanocomposites for additive

manufacturing applications. Quantum dots – crystalline semiconducting nanoparticles – have been utilized for a number of applications including solar cells,[20,21] biological tagging,[22] lighting/displays,[23,24] and mechanical load sensing applications,[25] but their use in additive manufacturing is still a relatively new area of study. Prior research has used ink-jet printing technologies to print quantum dot structures on a relatively small scale,[26,27] but the approach we demonstrate here allows for the direct incorporation and implementation of quantum dots within additive manufacturing processes enabling the production of large-scale structures and parts. The basis of our approach is the process of incorporating cadmium sulfur selenide graded alloy quantum dots (CdSSe QDs) within a polylactic acid (PLA) host matrix through solution-based mixing to extrude printer filament. Many tests and material characterizations are performed to reveal the overall effects that functionalization has on the properties of the embedded quantum dots and polymer host matrix as well as the mechanisms that control these effects. To demonstrate the ability to additively manufacture components exhibiting new material behaviors, light pipes and fluorescent devices are printed using a FDM approach by harnessing the optical response of embedded CdSSe graded alloy quantum dots within the 3D printing process. The development of quantum dot-functionalized 3D printer filament represents a unique opportunity for the advancement and design of new materials compatible with additive manufacturing processes and applications.

EXPERIMENTAL

Chemicals and Materials

Cadmium Oxide (CdO, 99.99%), octadecene (ODE, 90%), oleic acid (OA, 90%), and tri-n-butylphosphine (TBP, 97% mixture of isomers) were purchased from Sigma Aldrich and used

without further modification. Elemental selenium (Se, 99.999%) was purchased from Alfa Aesar and sulfur powder (USP sublimed) was purchased from Fischer Scientific. ACS grade dichloromethane and toluene solvents were purchased from Fischer Scientific. Polylactic acid pellets (3D850) were purchased from Filabot and supplied by Natureworks.

Synthesis of graded alloy Cadmium Sulfur Selenide Quantum Dots

Cadmium sulfur selenide graded alloy quantum dots (CdSSe QDs) were synthesized according to the protocol presented by Keene et al.[28] In short, the synthesis proceeded as follows: 4 mmol CdO and 16 mmol OA were mixed with 80 ml ODE in a 250 mL round bottom flask and heated with stirring to 300°C under inert atmosphere conditions. Once the solution was clear and colorless, a mixture of 2.24 mL 0.75 M S/TBP/ODE and 0.96 mL 0.75 M Se/TBP/ODE was quickly injected. Following injection, the reaction was further heated at 260°C under stirring for two hours, upon which the solution was cooled using compressed air. CdSSe QDs were cleaned through centrifugation for 15 min at 7500 RPM in a butanol/ethanol mixture (3:2 ratio by volume), resuspended in toluene and run through a column of poly(styrene-co-divinylbenzene).[29]

Filament and Sample Fabrication

PLA/CdSSe QD nanofunctionalized filament was fabricated through pre-mixing and dissolution of CdSSe QDs and PLA according to previously reported protocols.[16] In short, a predetermined amount of PLA pellets were dissolved in dichloromethane under stirring. Following complete dissolution, CdSSe QDs in toluene were added to the solution to obtain the desired weight percent in PLA (i.e. 0% (pure PLA), 0.1%, 0.5%, 1%, 3%, 5%, 7% CdSSe QDs in PLA

by weight). The PLA/CdSSe QD mixture was then further stirred to ensure the quantum dots were evenly dispersed in the PLA matrix. The resulting PLA/CdSSe QD nanocomposite was dried overnight to remove excess solvent and the remaining hard plastic was shredded to obtain small pellets. A Filabot EX2 single screw material extrusion system, heated to 180°C, was used to extrude PLA/CdSSe QD functionalized filament. Filament, approximately 2.85 mm in diameter, was cooled, spooled and ready to be used for printing.

An Ultimaker 3+ extended dual nozzle FDM type 3D printer was used to fabricate all test samples studied in this report. Filament was extruded through a 0.4 mm print nozzle heated to 215°C and deposited on a heated build plate set at 60°C. All test samples were printed with a 1 mm print layer height and 100% material infill.

Characterization

Optical, thermal and mechanical testing and characterization were performed as follows. Absorbance measurements for CdSSe QDs in solution and PLA/CdSSe QD thin film samples were recorded in the visible range from 400 – 800 nm using a Cary 60 UV-Vis spectrophotometer and accompanying software with a scan rate of 4800 nm/min. A total of nine scans, recorded at three distinct locations from three individual 3D-printed films, were analyzed and averaged to obtain absorbance data for 3D-printed PLA/CdSSe QD thin films. Photoluminescence (PL) intensity measurements were recorded using a PTI spectrofluorometer with an excitation wavelength of 500 nm. A custom stand was used to support PLA/CdSSe QD films to ensure uniform orientation and positioning between individual scans. Averages and resultant standard deviations for PL scans were recorded from three samples for each concentration of quantum dots in PLA studied.

Transmission and scanning transmission electron microscopy (TEM/STEM) images for CdSSe QDs in solution and 3D-printed PLA/CdSSe QD films were recorded using a Technai Osiris electron microscope. CdSSe QD solution was dropcast onto a carbon-coated mesh grid, and the residual solvent was allowed to evaporate prior to imaging. Polymer samples were microtomed to obtain thin slices of PLA/CdSSe QD samples, approximately 75 nm in thickness, which were then supported on a nickel grid prior to imaging. All TEM grids were provided by TED Pella, Inc. STEM images and corresponding quantum dot sizes were analyzed using ImageJ software.

Thermogravimetric analysis was performed using a TGA Instrument Specialists TGA 1000 under nitrogen purge (100 mL/min). Samples were heated from 25°C to 500°C, and the corresponding residual weight loss was monitored for each weight percent of PLA/CdSSe QD tested. Differential scanning calorimetry (DSC) testing was performed using a TA Instruments Q 2000 under nitrogen purge (50 mL/min). Samples were equilibrated at -25°C and heated to 225°C at a rate of 25°C/min where the temperature was held isothermally for 5 min before being cooled back to -25°C. A total of three scans were run for each sample, and corresponding thermal data were recorded from the final scan. Averages and standard deviations were calculated from three samples for each weight percent of PLA/CdSSe QD tested.

Mechanical testing was performed using and Instron 5400 bench top load frame tensile testing system. 3D-printed ASTM D638 Type V tensile dogbone specimen were loaded at a rate of 5 mm/min under displacement control. A minimum of three tensile specimens were averaged to obtain the data presented here. All samples were observed to break within their gauge length during tensile testing.

Optical testing for the 3D-printed light pipe device was conducted using a 5 mW OBIS fiber-optic pig-tailed laser excitation source emitting at a wavelength of 405 nm, and the corresponding emission spectrum was recorded using a CDS 600 CCD-based spectrometer and accompanying software with an integration time of 2 s.

RESULT AND DISCUSSION

Optical properties of 3D-printed PLA/CdSSe QD nanocomposites

As synthesized CdSSe QDs, with a diameter of 5.7 $\pm$ 1.0 nm that was confirmed through TEM measurements (Figures 1 and S1), displayed an average quantum yield of 54% with a band-edge absorbance peak near 569 nm and a maximum photoluminescence (PL) emission intensity at 593 nm in solution (Figure 2). Polylactic acid, a thermoplastic polymer, was selected as the host matrix to fabricate functionalized filament due to its mutual solubility with CdSSe QDs in solution, minimal absorbance and emission across the visible spectra, ease of material processing and overall compatibility with material extrusion and fused deposition modeling type 3D-printing systems.[16]

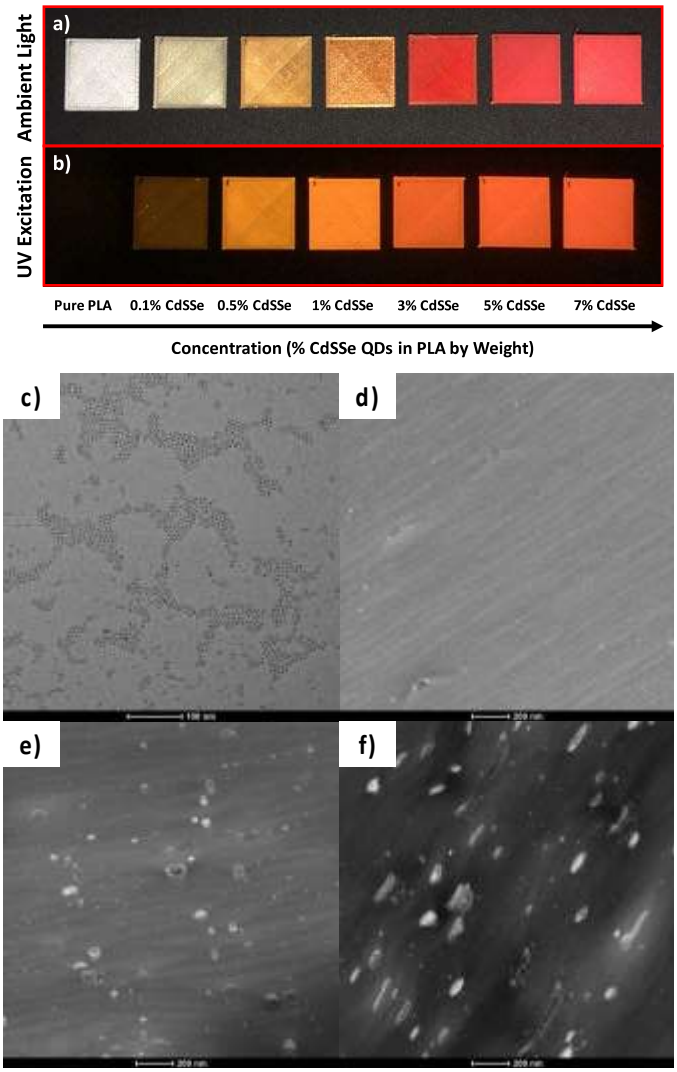

Figure 1. 3D-printed pure PLA and PLA/CdSSe QD films at varying concentrations of CdSSe QDs in PLA by weight under a) ambient light and b) UV excitation (picture was taken using a UV filter). Corresponding TEM image of c) CdSSe QDs drop cast from solution (approximately 5.7 $\pm$ 1.0 nm in diameter, scale bar 100 nm), high angle annular dark field (HAADF) STEM images of d) PLA/CdSSe QD 3D-printed film (0.5% CdSSe QD in PLA by weight, scale bar 200 nm), e) PLA/CdSSe QD 3D-printed film (3% CdSSe QD in PLA by weight, scale bar 200 nm), f) PLA/CdSSe 3D-printed film (7% CdSSe QD in PLA by weight, scale bar 200 nm). Aggregation between individual quantum dots can be seen at increasing concentrations of CdSSe QDs in PLA.

Thin film templates, 0.5 mm in thickness, were fabricated to study the optical properties and characteristics of 3D-printed PLA/CdSSe QD samples at varying concentrations of CdSSe QDs in PLA by weight (Figure 1a and 1b). When incorporated within PLA, the absorbance behavior of CdSSe QDs remained relatively unchanged, as both the overall spectra and absorbance peak location for 3D-printed films were consistent with CdSSe QDs in solution following materials processing and printing (Figure 2a and 2b, respectively). Consistent with Beer-Lambert's Law for nanoparticles in solution, 3D-printed PLA/CdSSe QD films also displayed a linear relationship between absorbance intensity (measured at the absorbance peak for CdSSe QDs in solution, i.e. 569 nm) and quantum dot concentration (% of CdSSe QDs in PLA by weight) for the 3D-printed samples studied (Figure 2c).

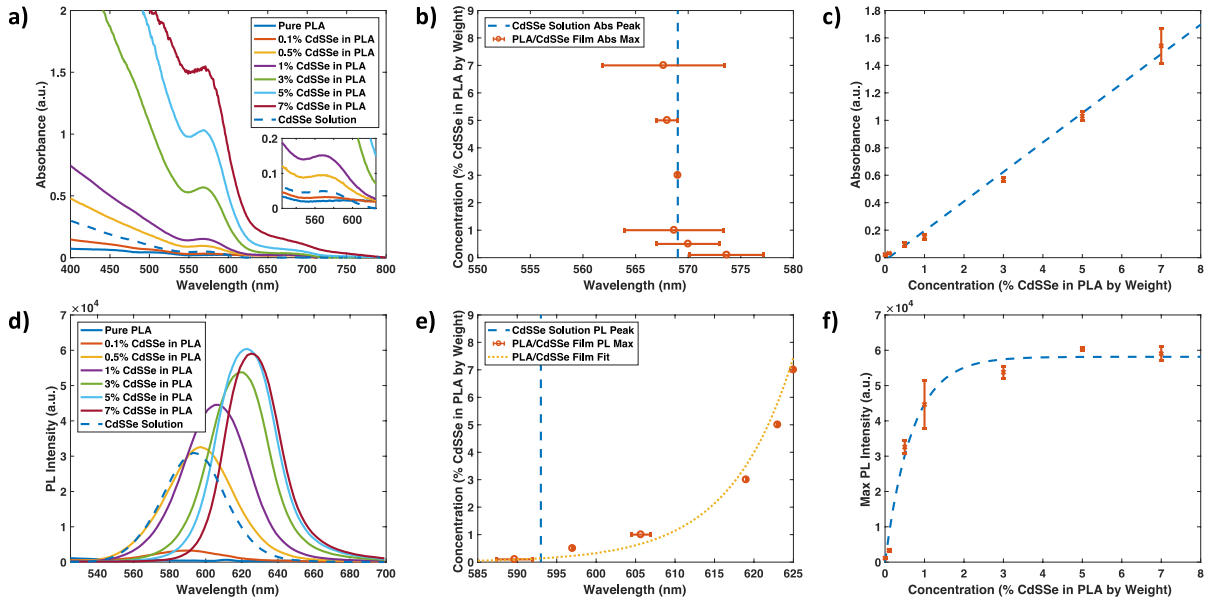

Figure 2. a) Average absorbance spectra of 3D-printed PLA/CdSSe QD films at varying concentrations of CdSSe QDs in PLA by weight and CdSSe QDs in solution. b) Location of absorbance peak for 3D-printed PLA/CdSSe QD films at varying concentrations of CdSSe QDs in

PLA by weight. c) Relationship between absorbance intensity (measured at absorbance peak for CdSSe QDs in solution, 569 nm) and concentration of CdSSe QDs in PLA by weight. d) Average photoluminescence spectra of 3D-printed PLA/CdSSe QD films at varying concentrations of CdSSe QDs in PLA by weight and CdSSe QDs in solution. e) Location of maximum photoluminescence for 3D-printed PLA/CdSSe QD films at varying concentrations of CdSSe QDs in PLA by weight. f) Relationship between maximum photoluminescence intensity and concentration of CdSSe QDs in PLA by weight.

The photoluminescence (PL) emission properties of 3D-printed PLA/CdSSe QD thin films were also evaluated. Though the overall monochromatic behavior of CdSSe QDs in solution was maintained following printing, a significant red shift in the location of maximum PL intensity was observed for increasing concentrations of CdSSe QDs in PLA (Figure 2d and 2e, respectively). For the highest concentration studied (7% CdSSe in PLA by weight), the location of maximum PL intensity was red-shifted by 32 nm relative to CdSSe QDs in solution. We attribute this spectral red shift to a combination of two factors previously illuminated in the literature: quantum dot aggregation in 3D-printed PLA/CdSSe QD films, and the presence of multiple size populations in the as-synthesized graded alloy CdSSe QDs enabling energy transfer from small to larger sized quantum dots in aggregated form.[30,31]

In order to quantify the degree to which quantum dot aggregation influenced the observed optical response, high angle annular dark field (HAADF) STEM images were recorded for 3D-printed PLA/CdSSe QD structures. According to prior research, we expect to see a direct relationship between aggregation and the recorded spectral shift.[30] At low concentrations (i.e. 0.5% CdSSe in PLA by weight), minimal aggregation was observed, and CdSSe QDs were well

dispersed throughout the 3D-printed structure (Figure 1d). Relative to CdSSe QDs in solution, the location for maximum PL emission was red-shifted by 4 nm for the 0.5% PLA/CdSSe QD 3D-printed sample (Figure 2e). At higher concentrations of CdSSe QDs in PLA (i.e. 3% and 7% CdSSe QDs in PLA by weight), though, distinct aggregation between individual quantum dots within the 3D-printed structures was confirmed (Figure 1e and 1f). In these samples, embedded CdSSe QDs existed primarily in larger, aggregated structures ranging in size from 49 ± 24 nm to 70 ± 54 nm, where the location of max PL intensity red shifted 26 nm and 32 nm for 3% and 7% CdSSe QDs in PLA by weight, respectively.

With increasing concentrations of embedded quantum dots and the resultant aggregation in 3D-printed PLA/CdSSe QD films, energy transfer between the multiple size populations in as-synthesized CdSSe QDs is expected to drive the observed spectral red shift (Figure 2d and 2e). This energy transfer, and corresponding reabsorption, is displayed by a narrowing of the full width at half maximum (FWHM) of the PL emission spectra for increasing concentrations of CdSSe QDs in PLA. Here, the lower wavelength emission associated with smaller quantum dots in the nanofunctionalized composite decreases, as its emission is reabsorbed by surrounding, larger CdSSe QDs, and the overall spectral response begins to be dominated by the higher wavelength component of the quantum dot emission (Figure S2). The spectral red shift observed for 3D-printed PLA/CdSSe QD films is expected to continue to plateau with increasing concentrations of quantum dots, as indicated by the trends obtained for the samples studied in this manuscript.

Similar to the observed spectral red shift, the overall PL intensity of 3D-printed PLA/CdSSe QD films was also found to be concentration dependent. Near a 3% by weight loading, PL intensity begins to reach a steady state for increasing concentrations of CdSSe QDs in PLA. These

results are similar to previously reported findings, where the emission intensity of ultra-small cadmium selenide quantum dots embedded within polymeric films began to approach a maximum value with increasing concentration of quantum dots.[32] We attribute these trends to aggregation in the 3D-printed structures, and a corresponding reduction in quantum efficiency of the aggregated quantum dots occurs due to their close proximity.

Beyond absorbance and emission characteristics, fluorescence lifetime measurements of CdSSe QDs in solution and 3D-printed PLA/CdSSe QD films were also evaluated. Decay curves were fit to a three-component exponential function, and the lifetimes of PLA/CdSSe QD films were found to be shorter than that of CdSSe QDs in solution (see Supporting Information). Again, this behavior can be attributed to the increase in aggregation and energy transfer between the multiple size populations present in the PLA/CdSSe QD 3D-printed samples (Figure S3).[33,34]

Thermal properties 3D-printed of PLA/CdSSe QD nanocomposites

The thermal stability of PLA/CdSSe QD nanocomposite systems was studied using thermogravimetric analysis. Residual weight versus temperature for 3D-printed pure PLA and PLA/CdSSe QD samples are shown in Figure S4. All samples, regardless of CdSSe QD concentration, displayed a single weight loss step beginning near 250°C, followed by complete material loss occurring above 350°C. With material extrusion/filament fabrication and 3D printing operating temperatures of 180°C and 215°C, respectively, thermogravimetric analysis confirms the thermal stability of PLA/CdSSe QD nanocomposites in the operating temperature range, and that minimal material degradation or loss occurs during both filament fabrication and 3D printing processes.

The thermal response of 3D-printed PLA/CdSSe QD nanocomposites was also studied using differential scanning calorimetry to better understand the behavior of the polymer chain network and overall impact that filament functionalization has relative to the unmodified PLA host matrix. Representative differential scanning calorimetry scans for 3D-printed pure PLA and PLA/CdSSe QD samples are shown in Figure 3a. Average values for glass transition temperature (T_g), crystallization temperature (T_c) and melting temperature (T_m) are plotted in Figure 3b and further detailed in Table S2. With increasing concentrations of CdSSe QDs in PLA, glass transition, crystallization and melting temperatures were observed to decrease relative to the unmodified pure PLA following materials processing and 3D printing, with more significant decreases in the recorded thermal transitions occurring at higher concentrations of CdSSe QDs in PLA (Figure 3b).

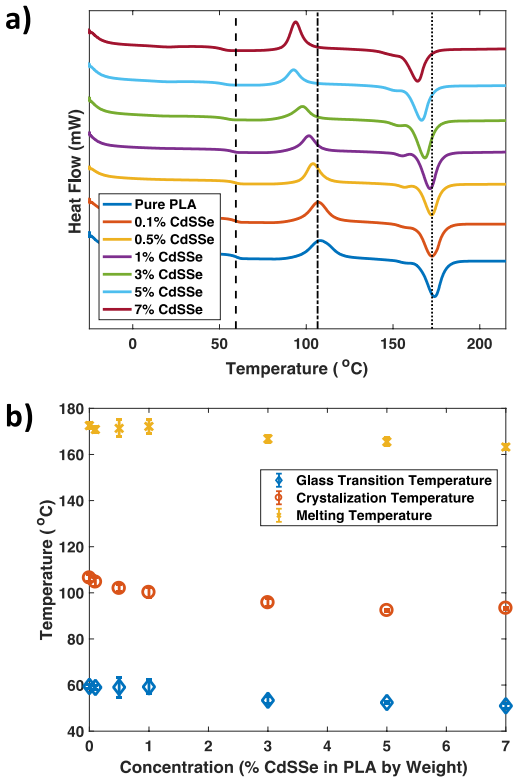

Figure 3. a) Representative differential scanning calorimetry curves for 3D-printed pure PLA and PLA/CdSSe QD samples at various concentrations of CdSSe QDs in PLA by weight. Dashed lines are guides for the eye and represent average values of pure PLA glass transition temperature, crystallization temperature and melting temperature, from left to right respectively. b) Average glass transition temperature, crystallization temperature and melting temperature for 3D-printed pure PLA and PLA/CdSSe QDs at various concentrations of CdSSe QDs in PLA by weight (data is further detailed in Table S2).

These changes in thermal transition can be attributed to a combination of two underlying mechanisms: 1) interactions between the PLA host matrix and natively bound surface ligands present on CdSSe QDs, and 2) aggregation and agglomeration between CdSSe QDs in the final 3D-printed structure. Surface ligand-polymer chain interactions are known to have a significant impact on the overall behavior of polymer-based nanocomposite systems. For attractive interactions, thermal transitions, namely glass transition temperature, are typically observed to increase when compared to the unmodified host matrix even at relatively high concentrations of embedded nanomaterials.[35] This behavior is due in part to embedded nanoparticles chemically interacting with and binding to the surrounding polymer host matrix, restricting polymer motion due to an increased energy barrier for intermolecular chain movement.[36] In the case of 3D-printed PLA/CdSSe QD nanocomposites, though, the opposite trend is observed. We attribute this behavior to poor interactions between the pure PLA chain network and oleic acid surface ligands present on the embedded CdSSe QDs (Figure S5). Fatty acids, such as oleic acid, consisting of a long hydrocarbon chain and terminal carboxyl group, have been previously reported to act as a plasticizing agents when incorporated within a pure PLA host matrix.[37] Plasticizing agents

are known to lower glass transition temperature, as well as crystallization and melting temperatures, by effectively allowing for improved polymer chain mobility and alignment.[38] We expect that the methyl-rich surface of the oleic acid-modified CdSSe QDs interacts weakly through Van der Waals forces with the PLA polymer chain network. As such, we hypothesize that the lack of strong intermolecular interactions between oleic acid and PLA results in the formation of additional free surfaces and free spaces near embedded quantum dots, as PLA is unable to adequately wet the surface of oleic acid-capped CdSSe QDs.

In addition to the aforementioned impact of native surface ligands, the size and concentration of embedded nanomaterials, including the presence of aggregates, has also been found to influence the overall thermal response of polymer-based nanocomposite systems.[39–41] As discussed previously, CdSSe QDs were observed to form aggregates in micelle-like structures at increasing concentrations of quantum dots in PLA (Figure 1). With weak chemical interactions between the surrounding polymer matrix, aggregated quantum dots can be thought of as acting as void spaces in the 3D-printed PLA/CdSSe QD nanocomposite systems. The presence of voids at nanoparticle-polymer interfaces have been found to reduce the glass transition behavior of polymer-based nanocomposite systems due to the resultant increased polymer mobility near the regions surrounding embedded nanomaterials.[36] Thermal transitions of 3D-printed PLA/CdSSe QD nanocomposites are expected to decrease with increasing aggregate size due to the formation of larger polymer chain discontinuities and the resultant formation of interphase regions near quantum dot surfaces resulting from weak polymer-nanoparticle interactions, consistent with the trends obtained in this study.[42]

Mechanical properties of 3D-printed PLA/CdSSe QD nanocomposites

The tensile load responses of 3D-printed pure PLA and PLA/CdSSe QD samples were studied to evaluate the impact of filament functionalization on the mechanical properties of as-printed PLA/CdSSe QD nanocomposites. The presence of CdSSe QDs in 3D-printed dogbone samples is visible under both ambient light, where samples maintained the orange coloration of CdSSe QDs in solution, and UV excitation, where the fluorescent behavior of the embedded quantum dots was preserved following materials processing and 3D printing (Figure S6). Representative stress vs. strain curves for 3D-printed pure PLA and PLA/CdSSe QD dogbone specimens loaded in tension are shown in Figure 4a. A summary of relevant mechanical testing results, including average ultimate tensile strength, average strain at break, as well as average elastic modulus and toughness for all samples tested is presented in Figure 4 and further detailed in Table S3.

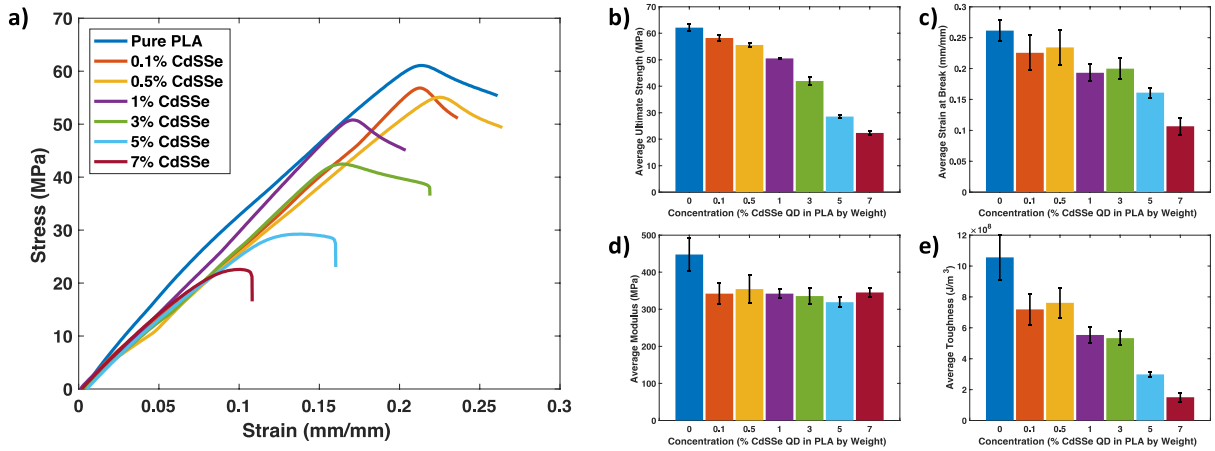

Figure 4. Tensile load response of 3D-printed pure PLA and PLA/CdSSe QD dogbone specimens. a) Representative stress vs. strain curves for varying concentrations of CdSSe QDs in PLA by weight. b) Average ultimate strength for varying concentrations of CdSSe QDs in PLA by weight. c) Average strain at break for varying concentrations of CdSSe QDs in PLA by weight. d) Average

modulus for varying concentrations of CdSSe QDs in PLA by weight. e) Average toughness for varying concentrations of CdSSe QDs in PLA by weight. Similar to the results obtained for differential scanning calorimetry testing, the mechanical load response of 3D-printed PLA/CdSSe QD specimens was found to be dependent on the overall concentration of embedded quantum dots. For the tensile dogbone specimens, ultimate strength, strain, modulus and toughness were all observed to decrease relative to pure PLA following the inclusion of CdSSe QDs within the 3D-printed structures. The largest decrease in material strength properties were, on average, observed for the highest concentrations of embedded quantum dots. In fact, ultimate strength and fracture toughness for PLA/CdSSe QD samples containing 7.0% quantum dots by weight were found to decrease by 63% and 85%, respectively, relative to the unmodified pure PLA matrix. We again attribute these changes in material strength properties to a combination of weak polymer-surface ligand interactions and quantum dot aggregation present in the final 3D-printed structures.

Upon initial inspection of the recorded thermal and mechanical testing results, the embedded quantum dots appear at first to be acting as a plasticizing agent. For polymer based systems, and PLA in particular, the addition of plasticizers has been shown to decrease both the ultimate tensile strength and tensile modulus, consistent with the results obtained for 3D-printed PLA/CdSSe QD samples.[43,44] By promoting intermolecular chain movement, plasticizers are also well known to cause increased deformation for thermoplastic materials. In the case of our 3D-printed PLA/CdSSe QD nanocomposite system, though, elongation at break was observed to decrease, resulting in a more brittle material response with increasing concentrations of

embedded quantum dots; this is the opposite effect of what is typically observed for plasticized polymer systems.

At low concentrations of embedded quantum dots (i.e. 0.1% and 0.5% CdSSe QDs in PLA), no statistical difference in the recorded strain response was observed relative to the unmodified pure PLA host matrix, as samples had overlapping standard deviations. These samples also displayed the smallest changes in recorded ultimate strength and toughness, as the low concentrations of embedded quantum dots have limited impact on the polymer chain network. The formation of aggregates and agglomerates in polymer-based nanocomposite structures, however, has been shown to significantly influence the underlying polymer structure and resulting thermal and mechanical behaviors. The presence of aggregates in a polymer matrix, such as those observed in 3D-printed PLA/CdSSe QD structures at higher concentrations of embedded quantum dots, can act as sites for crack initiation and propagation that ultimately lead to the premature and brittle failure of nanocomposite systems.[45] The combined contribution of aggregation and the overall lack of interaction between oleic acid-capped CdSSe QDs and surrounding PLA host matrix significantly reduces the ability of 3D-printed PLA/CdSSe QD nanocomposites to carry mechanical load. The resultant outcome is a decreased ultimate tensile strength and strain at failure, where aggregated quantum dots ultimately form representative void spacings within the PLA host matrix.

The impact of quantum dot functionalization on the recorded modulus and toughness of PLA/CdSSe QD samples should also be noted. Modulus is commonly defined as the ability of a material to deform elastically under the application of external load, and it offers a means to measure corresponding stiffness of the material. Modulus for PLA/CdSSe QD samples was

recorded directly during tensile testing as the slope of the linear component of the stress-strain curve (Figure 4a). Following the addition of CdSSe QDs to the PLA host matrix, a decrease in the recorded modulus was observed. Unlike other thermal and mechanical testing results, modulus did not appear to be dependent upon the overall concentration of embedded quantum dots. Rather, a single drop in modulus of approximately 25% relative to unmodified pure PLA was observed. These results are in line with previously reported polymer-nanocomposite systems where increased polymer chain mobility due to the presence of embedded nanomaterials resulted in a decreased modulus due to the lack of intermolecular interactions present at the surface of the embedded quantum dots.[46,47]

Toughness was calculated as the integral under the stress-strain curve, and the integral correlates to the ability of a material to absorb energy when loaded. Typically, ductile materials are thought of as being 'tougher' as they are able to absorb energy over longer periods of time due to increased elongation before failure. With increasing concentration of CdSSe QDs in PLA, a significant decrease in material toughness was observed. In line with the reduced ultimate strength and strain at failure, material toughness decreases in accordance with the overall concentration of embedded quantum dots. This reduction in capacity to absorb energy results from quantum dot aggregation and a corresponding inability to carry load due to the poor intermolecular interactions between the CdSSe QDs and the surrounding PLA matrix.[46]

3D-printed PLA/CdSSe QD light devices

In order to demonstrate a significant potential application for 3D-printed PLA/CdSSe QD nanocomposite systems, hollow U-shaped optical light pipes were fabricated (Figures 5a and 5b).[48] Light pipes are components and devices that are used to transport or redirect light from a

source to a desired location.[49] Proof-of-concept light pipes were 3D-printed using an inner shell of PLA/CdSSe QD functionalized material (0.5% and 3.0% CdSSe QDs in PLA by weight), surrounded by a white PLA exterior to aid with internal reflection of the quantum dot emission. Although the light pipe does not currently operate using total internal reflection, it is believed to transport light through a combination of reflection and scattering. Further studies are to be completed in order to increase the amount of internal reflection in the 3D-printed device. Methods to achieve this goal will focus on printing a surrounding layer with a higher refractive index polymer than the PLA, or to coat the PLA/CdSSe QD layer with a reflective material. When excited with an external emission source, a red shift in the location of maximum PL emission relative to quantum dots in solution was observed for the light pipe devices tested, similar to trends observed for PLA/CdSSe QD thin film samples discussed previously (Figure 5c). Opposite from the trends displayed for 3D-printed PLA/CdSSe QD thin films, though, the PL emission intensity for the optical light pipe was observed to decrease with increasing concentration of embedded quantum dots (i.e. as the weight percent of CdSSe QDs in PLA increased from 0.5% to 3.0%). We attribute this behavior to the attenuation of quantum dot emission due to the increased number of quantum dots absorbing light in the 3.0% PLA/CdSSe QD light pipe as compared to the 0.5% PLA/CdSSe QD light pipe.[50] Additionally, as the thickness of the PLA/CdSSe QD inner layer was reduced, the recorded PL emission intensity was observed to decrease (Figure 5d). This trend is attributed to the decrease in absorption cross-section and corresponding reduction in the overall number of quantum dots along the excitation path. By tuning the size, concentration and type of embedded quantum dots, as well as the thickness of the inner

quantum dot-functionalized layer, a customized optical light pipe with tunable emission wavelength and intensity can be obtained by 3D-printing.

Additionally, as a second example of a representative application for 3D-printed light device, a Vanderbilt logo was printed using PLA/CdSSe QD filament encased within a white PLA surround (Figures 5e and 5f). This device represents the capability of 3D-printing to fabricate bulk-scale fluorescent displays and devices using multiple materials.

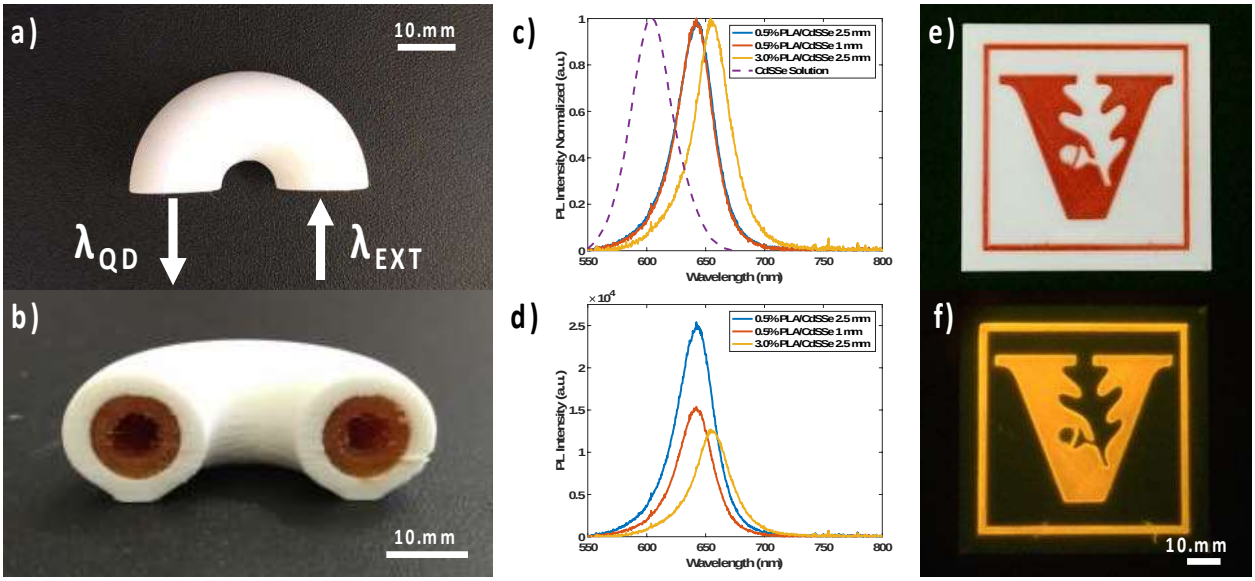

Figure 5. 3D-printed optical light pipe. a) Top view. b) Profile view, thickness of interior PLA/CdSSe QD layers tested was 1 mm and 2.5 mm, respectively. c) Normalized PL spectra for CdSSe QD solution and 3D-printed PLA/CdSSe QD optical light pipes. d) PL spectra for 3D-printed PLA/CdSSe QD optical light pipes. e) 3D-printed fluorescent device under ambient light. f) 3D-printed fluorescent device under UV excitation (picture was taken using a UV filter).

Conclusions

In this work, we successfully demonstrate the ability to develop functionalized nanocomposite materials compatible with 3D printing applications through the incorporation of CdSSe QDs within a PLA host matrix. Focusing on materials processing considerations, CdSSe QDs and PLA are mixed, dried and extruded to obtain filament compatible with stock fused deposition modeling (FDM) type 3D printers. The optical, thermal and mechanical responses of 3D-printed CdSSe QD structures were studied to evaluate the impact that filament functionalization has relative to the unmodified PLA host matrix. While the overall absorbance behavior of CdSSe QDs was maintained following printing, slight changes in the photoluminescent behavior was observed for 3D-printed CdSSe QD structures. Most noticeable was the red shift in maximum PL emission intensity for increasing concentrations of embedded CdSSe QDs. We attribute this spectral shift to a combination of aggregated quantum dots within the 3D-printed structures and corresponding reabsorption resulting from multiple size populations within embedded quantum dots. The thermal and mechanical behaviors of 3D-printed PLA/CdSSe QD test specimens were also found to be dependent on the overall concentration of embedded quantum dots. In this case, reductions in thermal transitions and material strength properties are attributed to the presence of aggregated quantum dots and the overall lack of interaction between the natively bound oleic acid surface ligands present on CdSSe QDs and the surrounding PLA host matrix. By tuning the surface composition of the quantum dot to promote favorable interactions with the polymer host matrix, future research will focus on the development of 3D-printed nanocomposite systems with enhanced optical and mechanical strength properties. The ability to incorporate quantum dots and other nanomaterials within 3D printing and additive manufacturing processes represents a unique opportunity for the design and development of

new materials and structures with advanced, multifunctional behaviors and properties for a variety of applications and uses.

AUTHOR INFORMATION

Conflicts of Interest

There are no conflicts of interests to declare.

Corresponding Authors

* Douglas Adams: douglas.adams@vanderbilt.edu
* Sandra Rosenthal: sandra.j.rosenthal@vanderbilt.edu

Author Contributions

All authors have given approval to the final version of the manuscript.
‡These authors contributed equally to this work.

Funding Sources

The Vanderbilt research team would like to acknowledge the support of the U.S. Department of Energy, which provided funding for the project under the support of the Nuclear Energy Enabling Technologies (NEET) Program, Award Number DE-NE0008712 as well as the support of the U.S. Office of Naval Research, which provided funding for this research as part of a Multi-Disciplinary University Research Initiative on Sound and Electromagnetic Interacting Waves under grant number N00014-10-1-0958.

Acknowledgments

The authors would like to acknowledge Dr. Ian Njoroge for his helpful insights and discussion, Devon Powers and Dr. Peter Pintauro for assistance and use of the differential scanning calorimetry system, and Brian O'Grady and Dr. Leon Bellan for access to the Instron load frame setup. We would also like to acknowledge the Vanderbilt Institute of Nanoscale Science and Engineering for access to the Technai Osiris transmission electron microscope. PLA/CdSSe QD TEM samples were prepared in part through the use of Vanderbilt Cell Imaging Shared Resource (supported by NIH grants CA68485, DK20593, DK58404, DK59637 and EY008126).

Supporting Information

Additional supporting information referenced in the paper can be found online.

References

1 F. Ning, W. Cong, J. Qiu, J. Wei and S. Wang, *Compos. Part B Eng.*, 2015, **80**, 369–378.
2 K. V. Wong and A. Hernandez, *ISRN Mech. Eng.*, 2012, **2012**, 1–10.
3 J. P. Kruth, *CIRP Ann. - Manuf. Technol.*, 1991, **40**, 603–614.
4 F. Calignano, D. Manfredi, E. P. Ambrosio, S. Biamino, M. Lombardi, E. Atzeni, A. Salmi, P. Minetola, L. Iuliano and P. Fino, *Proc. IEEE*, 2017, **105**, 593–612.
5 T. J. Horn and O. L. A. Harrysson, *Sci. Prog.*, 2012, **95**, 255–282.
6 B. Berman, *Bus. Horiz.*, 2012, **55**, 155–162.
7 S. J. Leigh, R. J. Bradley, C. P. Purssell, D. R. Billson and D. A. Hutchins, *PLoS One*, 2012, **7**, e49365.
8 Z. Xun Khoo, J. Ee Mei Teoh, Y. Liu, C. Kai Chua, S. Yang, J. An, K. Fai Leong and W. Yee Yeong, 2015, **103**, 103–122.
9 C. L. Ventola, *P T*, 2014, **39**, 704–711.
10 P. Dudek, *Arch. Metall. Mater.*, 2013, **58**, 1415–1418.
11 P. C. Lebaron, Z. Wang and T. J. Pinnavaia, *Appl. Clay Sci.*, 1999, **15**, 11–29.
12 R. Kasemann and H. Schmidt, *New J. Chem.*, 1994, **18**, 1117–1123.
13 L. L. Beecroft and C. K. Ober, *Chem. Mater.*, 1997, **9**, 1302–1317.
14 Z. Weng, J. Wang, T. Senthil and L. Wu, *Mater. Des.*, 2016, **102**, 276–283.
15 Z. C. Kennedy, J. F. Christ, K. A. Evans, B. W. Arey, L. E. Sweet, M. G. Warner, R. L. Erikson and C. A. Barrett, *Nanoscale*, 2017, **9**, 5458–5466.
16 C. D. Brubaker, M. A. Davies, J. R. McBride, S. J. Rosenthal, G. Kane Jennings and D. E. Adams, *Appl. Nano Mater.*, 2018, **1**, 1377–1384.
17 M. R. Skorski, J. M. Esenther, Z. Ahmed, A. E. Miller and M. R. Hartings, *Sci. Technol. Adv. Mater.*, 2016, **17**, 89–97.
18 D. Zhang, B. Chi, B. Li, Z. Gao, Y. Du, J. Guo and J. Wei, *Synth. Met.*, 2016, **217**, 79–86.
19 Q. Zhang, F. Zhang, S. P. Medarametla, H. Li, C. Zhou and D. Lin, *Small*, 2016, **12**, 1702–1708.
20 E. H. Sargent, *Nat. Photonics*, 2012, **6**, 133–135.
21 J. S. Niezgoda, E. Yap, J. D. Keene, J. R. Mcbride and S. J. Rosenthal, *Nano Lett.*, 2014, **14**, 3262–3269.
22 O. Kovtun, D. Sakrikar, I. D. Tomlinson, J. C. Chang, X. Arzeta-Ferrer, R. D. Blakely and S. J. Rosenthal, *ACS Chem. Neurosci.*, 2015, **6**, 526–534.
23 Y. Yang, Y. Zheng, W. Cao, A. Titov, J. Hyvonen, J. R. Manders, J. Xue, P. H. Holloway and L. Qian, *Nat. Photonics*, 2015, **9**, 259–265.
24 T.-H. Kim, K.-S. Cho, E. K. Lee, S. J. Lee, J. Chae, J. W. Kim, D. H. Kim, J.-Y. Kwon, G. Amaratunga, S. Y. Lee, B. L. Choi, Y. Kuk, J. M. Kim and K. Kim, *Nat. Photonics*, 2011, **5**, 176–182.
25 C. D. Brubaker, T. M. Frecker, I. Njoroge, D. O. Shane, C. M. Smudde, S. J. Rosenthal, G. K. Jennings and D. E. Adams, 2016, **9803**, 980316.
26 Y. L. Kong, I. a Tamargo, H. Kim, B. N. Johnson, M. K. Gupta, T. W. Koh, H. A. Chin, D. a Steingart, B. P. Rand and M. C. McAlpine, *Nano Lett.*, 2014, **14**, 7017–7023.
27 Q.-H. Zhang, Y. Tian, C.-F. Wang, S. Chen, L. Li, J. Herbich, B. Golec, I. Wielgus, A. Pron, X. J. Wei, S. G. Wang, J. T. Zhang, Y. Du, S. X. Dou and H. S. Zhu, *RSC Adv.*, 2016, **6**, 47616–47622.
28 J. D. Keene, J. R. McBride, N. J. Orfield and S. J. Rosenthal, *ACS Nano*, 2014, **8**, 10665–

10673.
29 Y. Shen, M. Y. Gee, R. Tan, P. J. Pellechia and A. B. Greytak, *Chem. Mater.*, 2013, **25**, 2838–2848.
30 M. Danek, K. F. Jensen, C. B. Murray and M. G. Bawendi, *Chem. Mater.*, 1996, **8**, 173–180.
31 M. A. Harrison, A. Ng, A. B. Hmelo and S. J. Rosenthal, *Isr. J. Chem.*, 2012, **52**, 1063–1072.
32 M. a. Schreuder, J. D. Gosnell, N. J. Smith, M. R. Warnement, S. M. Weiss and S. J. Rosenthal, *J. Mater. Chem.*, 2008, **18**, 970.
33 J. Xu, J. Wang, M. Mitchell, P. Mukherjee, M. Jeffries-El, J. W. Petrich and Z. Lin, *J. Am. Chem. Soc.*, 2007, **129**, 12828–12833.
34 C. R. Kagan, C. B. Murray, M. Nirmal and M. G. Bawendi, *Phys. Rev. Lett.*, 1996, **76**, 1517–1520.
35 P. Rittigstein and J. M. Torkelson, *J. Polym. Sci. Part B Polym. Phys.*, 2006, **44**, 2935–2943.
36 B. J. Ash, R. W. Siegel and L. S. Schadler, *J. Polym. Sci. Part B Polym. Phys.*, 2004, **42**, 4371–4383.
37 M. Belgacem and A. Gandini, *Monomers, polymers and composites from renewable resources*, Elsevier Science, Amsterdam, 1st edn., 2008.
38 O. Martin and L. Averous, *Polymer (Guildf).*, 2001, **42**, 6209–6219.
39 R. Qiao, H. Deng, K. W. Putz and L. C. Brinson, *J. Polym. Sci. Part B Polym. Phys.*, 2011, **49**, 740–748.
40 T. Ramanathan, H. Liu and L. C. Brinson, *J. Polym. Sci. Part B Polym. Phys.*, 2005, **43**, 2269–2279.
41 L. Hamming, R. Qiao, P. Messersmith and L. Brinson, *Compos. Sci. Technol.*, 2009, **69**, 1880–1886.
42 A. Bansal, H. Yang, C. Li, K. Cho, B. C. Benicewicz, S. K. Kumar and L. S. Schadler, *Nat. Mater.*, 2005, **4**, 693–698.
43 M. Baiardo, G. Frisoni, M. Scandola, M. Rimelen, D. Lips, K. Ruffieux and E. Wintermantel, *J Appl Polym Sci*, 2003, **90**, 1731–1738.
44 I. Pillin, N. Montrelay and Y. Grohens, *Polymer (Guildf).*, 2006, **47**, 4676–4682.
45 B. J. Ash, D. F. Rogers, C. J. Wiegand, L. S. Schadler, R. W. Siegel, B. C. Benicewicz and T. Apple, *Polym. Compos.*, 2002, **23**, 1014–1025.
46 W. Xu, S. Raychowdhury, D. D. Jiang, H. Retsos and E. P. Giannelis, *Small*, 2008, **4**, 662–669.
47 J. Y. Lee, K. E. Su, E. P. Chan, Q. Zhang, T. Emrick and A. J. Crosby, *Macromolecules*, 2007, **40**, 7755–7757.
48 B. M. Boyle, T. A. French, R. M. Pearson, B. G. McCarthy and G. M. Miyake, *ACS Nano*, 2017, **11**, 3052–3058.
49 J. F. Van Derlofske, *Proc. SPIE*, 2001, **4445**, 119–129.
50 I. Surez, H. Gordillo, R. Abargues, S. Albert and J. Martínez-Pastor, *Nanotechnology*, 2011, **22**, 435202.

Table of Contents Artwork

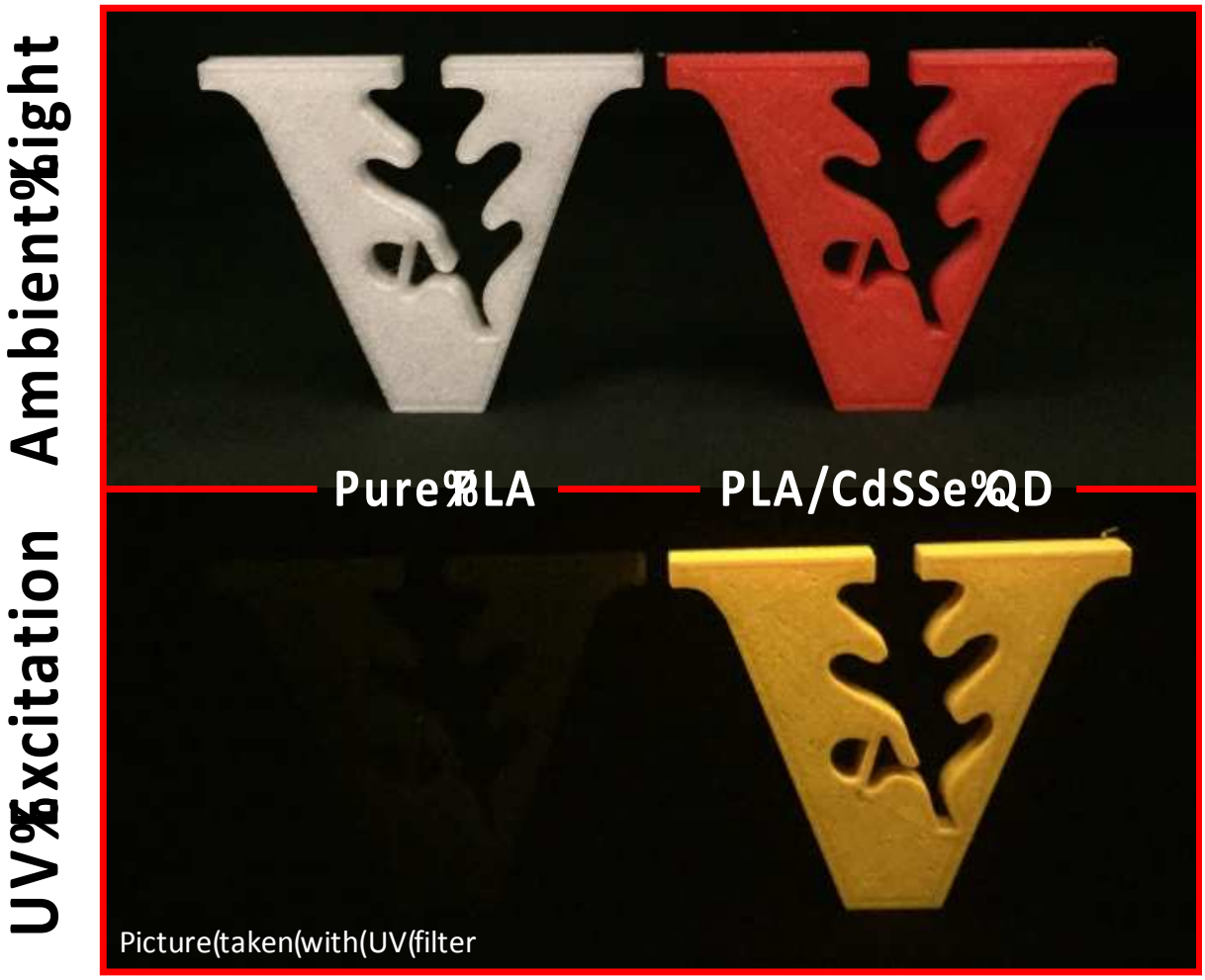

3D printing of Cadmium Sulfur Selenide quantum dot functionalized materials compatible with fused deposition modeling type processes and applications.